Available online at www.sciencedirect.com
SCIENCE DIRECT®
International Journal of Heat and Mass Transfer 49 (2006) 1358–1374
International Journal of HEAT and MASS TRANSFER
www.elsevier.com/locate/ijhmt

An analytical model for laser drilling incorporating effects of exothermic reaction, pulse width and hole geometry

G.K.L. Ng [a,*], P.L. Crouse [b], L. Li [b]

[a] TWI Technology Centre (Yorkshire), P.O. Box 3314, Sheffield S13 9WZ, UK
[b] Laser Processing Research Centre, School of Mechanical, Aerospace and Civil Engineering, The University of Manchester, P.O. Box 88, Manchester M60 1QD, UK

Received 21 June 2005
Available online 23 November 2005

Abstract

An analytical model is presented which incorporates the effects of using O_2 as assist gas. The contribution of the enthalpy of oxidation used in the model was determined experimentally by capturing the ejected melt and measuring the volume percentage of oxidation. The formulation of recoil pressure used in the model takes into account hole diameter and depth, and the associated pressure variation. The model presented also considers pulse width which is shown to affect the drilling velocity. The model enables the prediction of the velocity of melt ejection, and the drilling rate, as well as the contributions of melt ejection and vapourisation to the overall drilling rate. The calculated drilling rates are in close agreement with the experimental results.

Keywords: Laser drilling; Analytical model; Melt ejection; Drilling rate; Laser oxidation; Exothermic reaction

1. Introduction

Laser drilling involves a number of physical processes, typically melting, vapourisation, heat transfer by radiation, convection and conduction, vapour and melt flow, droplet formation and condensation of the vapour, absorption and reflection of electromagnetic radiation. Numerous models related to laser drilling have emerged over the last 40 years [1–33]. Before the current availability of inexpensive computing power, the emphasis was on finding solutions of appropriately simplified models. Early work by various researchers was mostly analytical in nature and laser drilling was modelled as a one-dimensional heat conduction problem [1,3,6]. This was adequate for low extraction efficiencies and low repetition rates, which allowed drilling of only shallow craters. Nevertheless, most of the one-dimensional models matched experimental drilling rates reasonably well. The capabilities of modern lasers have increased dramatically, and holes with aspect ratios beyond 10 can be easily drilled. The facts that analytical solutions are not available for moving-boundary phase-change problems, that actual geometries can be very complex, that the physical properties are invariably temperature-dependent, and that computer power has become very inexpensive have shifted current emphasis to numerical solutions. In recent years, there continues a growing number of one-dimensional models, with an ever-increasing development of higher-dimensional numerical models published in the open literature [8,9,12,30]. These models include both steady state and transient conditions and evaluate the effects of varying laser parameters on the temperature profile [21,22], removal rate and drilling speed [18,27–29,31] and the shape of the hole profile [11,12,20,28].

The model developed by Semak and Matsunawa [23] and later adapted to include the effects of using an O_2 assist gas for laser drilling by Low et al. [33], are both integral, steady-state, analytical models using mass and energy conservation as basis. The main thrust of the Semak and

* Corresponding author. Tel.: +44 114 2699046; fax: +44 114 2699781.
E-mail address: gary.ng@twi.co.uk (G.K.L. Ng).

0017-9310/$ - see front matter © 2005 Elsevier Ltd. All rights reserved.
doi:10.1016/j.ijheatmasstransfer.2005.10.002

Nomenclature

a	pre-exponential fitting parameter for friction factor
A	numerical coefficient
A_{eff}	effective area of assist gas flow (m^2)
A_{rl}	cylindrical area of radial loss of assist gas pressure (m^2)
b	exponential fitting parameter for friction factor
B_0	vapourisation constant (kg m^{-2})
C_{c}	constant for forced convection
$C_{p,\text{m}}$	specific heat of melt ($\text{J kg}^{-1}\text{ K}^{-1}$)
$C_{p,\text{s}}$	specific heat of solid ($\text{J kg}^{-1}\text{ K}^{-1}$)
d	hole diameter (m)
d_{n}	nozzle exit diameter (m)
f_{g}	assist gas flow rate ($\text{m}^3\text{ s}^{-1}$)
f_{vap}	friction factor of metal vapour
$\widehat{F}$	power per unit mass required to overcome frictional forces (W kg^{-1})
g	gravitational acceleration (9.8 m s^{-2})
h	heat transfer coefficient ($\text{W m}^{-2}\text{ K}^{-1}$)
I_{abs}	absorbed laser intensity (W m^{-2})
k_{b}	Boltzmann's constant ($1.38\times10^{-23}\text{ J K}^{-1}$)
k_{g}	thermal conductivity of assist gas ($\text{W m}^{-1}\text{ K}^{-1}$)
k_{s}	thermal conductivity of solid material ($\text{W m}^{-1}\text{ K}^{-1}$)
L	hole depth (m)
L_{m}	latent heat of melt (J kg^{-1})
L_{v}	latent heat of vapourisation (J kg^{-1})
m_{m}	mass of molten material ejected (kg)
m_{ox}	mass fraction of metal in alloy
$m_{\text{ox},i}$	mass fraction of ith metal in alloy
m_{s}	total mass of material removed (kg)
m_{v}	mass of material vapourised (kg)
$\dot{m}_{\text{v}}$	mass flow rate of vapourised material (kg s^{-1})
M_{m}	molar mass (kg mol^{-1})
$M_{\text{r,ox}}$	relative atomic mass of oxidising element (kg mol^{-1})
$M_{\text{r,ox},i}$	relative atomic mass of the ith oxidising element (kg mol^{-1})
n	number of mole
n_{c}	constant for forced convection
p_{c}	pressure of assist gas at the critical state (N m^{-2})
p_{r}	recoil pressure (N m^{-2})
p_{eff}	effective static assist gas pressure (N m^{-2})
p_i	nozzle pressure (N m^{-2})
P_{cond}	power lost to conduction (W)
P_{conv}	power lost to forced convection (W)
P_{in}	input power (W)
P_{melt}	power required for heating and melting (W)
P_{out}	output power (W)
Pr	Prandtl number
P_{r}	power from chemical reactions (W)
$P_{\text{r,ox}}$	heat generation rate due to oxidation of a particular element (W)
P_{vap}	power required for vapourisation (W)
p_{vap}	vapour pressure (N m^{-2})
q	convective cooling rate per unit area (J)
r_{l}	laser beam radius (m)
R	gas constant ($8.314\text{ J mol}^{-1}\text{ K}^{-1}$)
Re	Reynolds number
R_{ox}	reaction rate (mol s^{-1})
t	time (s)
T	absolute temperature (K)
T^*	average temperature within melt layer (K)
T_0	initial temperature of material (K)
T_{i}	temperature of assist gas inside nozzle (K)
T_{m}	melting point of solid material (K)
T_{s}	melt surface temperature (K)
T_{vap}	vapourisation temperature (K)
U	$(M_{\text{a}}L_{\text{v}})/N_{\text{a}}k_{\text{b}})$ (K)
v_{g}	gas flow velocity (m s^{-1})
v_{v}	velocity of the vapour (m s^{-1})
V_0	a constant (of the order of the speed of sound in the condensed phase)
V_{d}	drilling velocity (m s^{-1})
V_{dm}	drilling velocity due to melt ejection (m s^{-1})
V_{dv}	drilling velocity due to vapourisation (m s^{-1})
V_{m}	melt ejection velocity (m s^{-1})
V_{v}	velocity of vapourisation front along the z-axis (m s^{-1})
$\widehat{w}$	mechanical power (W)
z_{n}	nozzle–workpiece distance (m)
α_{c}	constant
α_{ox}	fraction of oxidised material
$\alpha_{\text{ox},i}$	fraction of ith oxidised material
γ	specific heat ratio
δ_{m}	thickness of melt layer (m)
κ_{m}	thermal diffusivity of melt ($\text{m}^2\text{ s}^{-1}$)
κ_{s}	thermal diffusivity of solid ($\text{m}^2\text{ s}^{-1}$)
μ_{g}	viscosity of assist gas ($\text{N m}^{-2}\text{ s}$)
μ_{v}	viscosity of vapour ($\text{N m}^{-2}\text{ s}$)
ρ	density (kg m^{-3})
ρ_{g}	density of assist gas (kg m^{-3})
ρ_{m}	melt density (kg m^{-3})
ρ_{s}	solid density (kg m^{-3})
ρ_{v}	vapour density (kg m^{-3})
σ	surface tension (N m^{-1})
ΔH_{ox}	enthalpy of oxidation (J mol^{-1})
$\Delta H_{\text{ox},i}$	enthalpy of oxidation for ith metal (J mol^{-1})
$\Delta_{\text{vap}}H$	enthalpy of vapourisation (J mol^{-1})
∇_{forward}	'forward' component of conduction term
∇_{radial}	'radial' component of conduction term

Matsunawa approach was to elucidate the effect of recoil pressure during the melt ejection process. The recoil pressure is taken to be due to the build-up of vapour pressure generated by surface heating. Low et al. extended the model by bringing in the effect of assist gas, adding two additional power terms, one for convective cooling and the other for exothermic reactions between the assist gas and molten phase, as well as by adding the pressure exerted by the assist gas to the recoil pressure. The model presented here further develops this approach and takes into account the fact that only a small percentage of the drilled material oxidises, and couples the vapour pressure at the drilled surface to the rate of vapour flow through the drilled hole; not previously considered. The new formulation of recoil pressure takes into account hole diameter and depth, bringing pressure variation into the model. Also, the contribution of the oxidation enthalpy is readdressed with the aid of experimental data.

2. Model description and assumptions

A schematic diagram to illustrate the model is given as Fig. 1. The laser beam impinges on the workpiece surface, is absorbed, and causes heating, melting and vapourisation. The recoil pressure generated by surface vapourisation, along with the pressure exerted by the assist gas, initiate radial ejection of the liquid melt from the interaction zone. When steady-state material removal is established, the drilling front propagates into the material at a drilling velocity determined by the absorbed laser intensity. The model ignores the initial melt ejection and addresses the processes taking place once the drilled hole reaches a finite depth. The total pressure causing melt ejection is taken to be the sum of the vapour pressure in the hole and the pressure exerted on the melt by the assist gas. The build-up of vapour pressure is relieved by the flow of the vapour through the drilled hole. Apart from aiding melt ejection, the assist gas can also add energy to the process if it reacts exothermally with the melt, typically oxygen forming metal oxides, or remove energy from the process by forced convective cooling.

In order to simplify the model the following assumptions were made:

1. Plasma generation was ignored. Only molten and vapour-phase metal are accounted for.
2. The metal vapour is assumed to be optically thin, thus absorbing none of the laser power.
3. Power absorption by the ejected melt is similarly ignored.
4. The generation of shock waves was assumed to be negligible.
5. The power distribution of the absorbed laser intensity, I_{abs}, is assumed to be uniform, and approximated by a top-hat profile.
6. The change in surface absorptivity due to oxide formation is ignored. The competing effects between the possible change in absorptivity of the surface due to oxide formation and the difference in the melting point of the oxide and metal considered, were assumed to cancel each other.
7. The impinging O_2 assist gas only interacts with the melt surface defined by the area covered by the spot size of the laser beam.
8. Not all the metal potentially available for oxidation, reacts with the oxygen assist gas, due to mass transfer constraints.
9. The metal vapour directly above the melt surface is in thermodynamic equilibrium with the metal surface.
10. The vapour pressure build-up above the melt surface is released by the vapour escaping through the drilled channel.

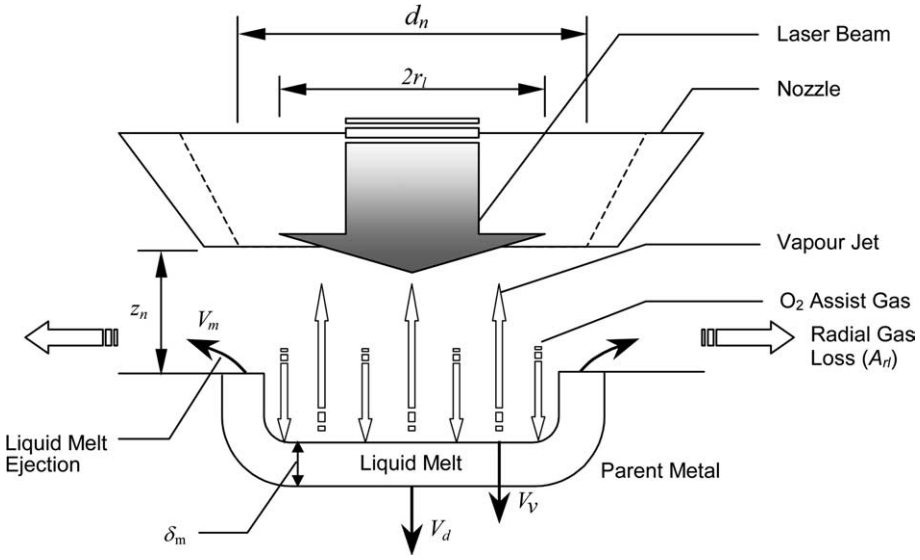

Fig. 1. Schematic diagram of the model with the use of an O_2 assist gas.

11. The combined effect of the vapour pressure build-up and assist gas pressure cause melt ejection. A high percentage of the melt is ejected, leaving a thin melt layer at the bottom of the hole, the thickness of which is inversely proportional to the drilling velocity.
12. Quasi-steady-state melt flow and propagation of the liquid–vapour and solid–liquid interfaces within the interaction zone were assumed, i.e. the propagation rate V_v of the vapourisation surface, the melt ejection velocity V_m, and the drilling velocity V_d are calculated from average values.

3. Mathematical formulation

3.1. Mass balance

On average during the drilling process the rate at which the solid metal melts is equal to the rate at which material is lost from the hole by vapourisation and melt ejection. Mathematically this is expressed as

$$\frac{dm_s}{dt} = \frac{dm_v}{dt} + \frac{dm_m}{dt} \tag{1}$$

Here m_s is the mass of metal melted, m_v is the mass of molten metal that is vapourised, m_m is the mass of molten metal that is ejected. Re-writing Eq. (1) for a hole diameter equivalent to the laser spot diameter of $2r_l$ one obtains

$$\pi r_l^2 \rho_s V_d = \pi r_l^2 \rho_m V_v + 2\pi r_l \delta_m \rho_m V_m \tag{2}$$

where V_v and V_m are the velocity of the vapourisation front and the melt ejection velocity respectively. One assumes that the melt front propagates with an average velocity, V_d, and that the average melt thickness can be approximated by

$$\delta_m \approx \frac{\kappa_m}{V_d} \tag{3}$$

where κ_m is the thermal diffusivity of the melt. Then by substituting Eq. (3) into Eq. (2) and rearranging one obtains

$$\rho_s V_d - \rho_m V_v - \frac{2\kappa_m \rho_m}{r_l V_d} V_m = 0 \tag{4}$$

The approach taken by both Semak and Matsunawa [23], and Low et al. [33], was to take the vapourisation velocity front, V_v, to be dependent on the melt surface temperature. Both used the following relationship, reworked from Frenkel [34], for calculating V_v

$$V_v = V_0 \exp\left(-\frac{U}{T_s}\right) \tag{5}$$

Here $U = (M_a L_v)/(N_a k_b)$, M_a and L_v are the atomic mass and latent heat of vapourisation of the metal respectively, N_a is the Avogadro's number, k_b is Boltzmann's constant and V_0 is a constant whose value is quoted to be of the order of the speed of sound in the condensed phase. It should be noted that Eq. (5) is derived solely from the energy distribution of the atoms in the solid, and no account is taken of the co-existing vapour phase beyond the surface, and the relationship between the boiling point and the vapour pressure is ignored.

Both Semak and Matsunawa [23], and Low et al. [33] calculated recoil pressure using the expression

$$p_r = A p_{vap}(T_s) = A B_0 T_s^{-\frac{1}{2}} \exp\left(-\frac{U}{T_s}\right) \tag{6}$$

A is a numerical coefficient and B_0 is a vapourisation constant. The value of the coefficient A is stated to vary between 0.55 for vapourisation in vacuum to unity for vapourisation under high ambient pressure. However, the derivation of Eq. (6) and of evaluating A appears not to be part of the open literature and is based on private communications.

The use of Eqs. (6) and (5) give very reasonable predictions for the values of the drilling velocity and melt ejection velocity, but leads to rather high predicted surface temperature values. In addition the two models mentioned do not take into account the depth of the drilled hole, and cannot account for differences in pulse width. For this latter reason, along with the desirability to use better-established theory, and to take account of pressure relief through vapour flow and the geometry of the drilled hole, a different approach was taken for calculating the velocity of the vapour front. Details are given in Section 3.5.

3.2. Melt ejection velocity

Assuming a uniform pressure profile within the laser beam (the result of the combined effect the of the vapour pressure and the assist gas pressure), the melt flow to be one-dimensional, and zero pressure to exist outside the beam, one can obtain an expression for the melt velocity, V_m, from Bernoulli's equation

$$p_{vap} + p_{eff} = \frac{\rho_m V_m^2}{2} + \rho_m g h + \frac{\sigma}{r_l} \tag{7}$$

The second and third terms on the right-hand side of Eq. (7) correspond to the hydrostatic and surface tension pressures respectively. Both terms are assumed to be negligible compared to the build-up of vapour pressure at the high-temperature surface, p_{vap}, and the assist gas pressure, p_{eff}. The melt ejection velocity is thus calculated from

$$p_{vap} + p_{eff} = \frac{\rho_m V_m^2}{2} \tag{8}$$

3.3. Vapour pressure

Vapour pressure can be directly calculated from the well-established Clausius–Clapeyron equation (e.g.) [35,36]:

$$p_{vap} = p_0 \exp\left[\frac{\Delta_{vap} H}{R}\left(\frac{1}{T_{vap}} - \frac{1}{T_s}\right)\right] \tag{9}$$

which relates surface temperature to vapour pressure. T_{vap} is the boiling point of the liquid at atmospheric pressure, p_0. The equation is derived by assuming thermodynamic equilibrium between the gas and the liquid phases, and allows for an increase of the boiling point should there be a pressure build-up. This expression is preferred to Eq. (6) used by both Semak and Matsunawa [23], and Low et al. [33]. The reason for this choice has already been given: the method for deriving Eq. (6) is not part of the open literature, and the exact functional dependence of the coefficient A on pressure is not known.

3.4. Assist gas pressure

It is well known that melt-ejection-dominated material removal is more efficient because the latent heat of vapourisation is much higher than the latent heat of fusion for metals. It is energy efficient to eject the molten material before excessive energy consumption by evaporation. Thus if a gas jet is used in tandem with the laser beam, material removal may be achieved with substantially lower laser power than by relying on the vapourisation-induced recoil pressure alone to expel the molten metal. As such, it is advised to introduce the effect of the pressure induced on the melt surface when an assist gas jet is used during laser drilling into the model.

It can be shown that for isentropic gas flow, the total pressure along a streamline is constant and equals the sum of the static and dynamic pressures. The total pressure is often called the stagnation pressure since it is the static pressure of the gas if its velocity was isentropically reduced to zero. The dynamic gas pressure can be neglected if the hole bottom is assumed to be perpendicular to the gas axis (Fig. 1) and if one assumes a uniform assist gas pressure profile within the laser beam and zero outside the beam. At the nozzle exit the gas has typically accelerated up to the local speed of sound leading to the critical state, indicated by the subscript 'c', due to adiabatic expansion of the gas [37]:

$$p_c = \left(\frac{2}{\gamma+1}\right)^{\frac{\gamma}{\gamma-1}} p_i \tag{10}$$

Here p_c is the pressure of assist gas at the nozzle exit, p_i is the pressure inside the nozzle. For diatomic gases such as O_2, the specific heat ratio, $\gamma = 1.4$.

For simplicity, the critical state is assumed to be found at the laser-drilled hole entrance, but with a reduced pressure due to the radial expansion of the gas outwards from the hole. The estimation of the reduced pressure is made by considering the geometrical areas of the gas flow entering the hole cavity and the gas flow which flows radially outwards as shown in Fig. 1 and expressed in the following equations:

$$A_{eff} = \pi r_l^2 \tag{11}$$

$$A_{rl} = d_n \pi z_n \tag{12}$$

Here A_{eff} is the effective area of flow entering the hole defined by the laser beam radius, r_l, (since zero assist gas pressure outside the beam was assumed), A_{rl} is the cylindrical area where the radial loss of gas pressure flows as defined by the nozzle exit diameter, d_n and nozzle–workpiece distance, z_n. As a result of these two flows, the assist gas pressure, p_c, at the nozzle exit is reduced to p_{eff} as follows:

$$p_{eff} = p_c \frac{A_{eff}}{A_{eff} + A_{rl}} = f(p_i) \tag{13}$$

where p_{eff} is the effective static gas pressure of the assist gas acting in the same direction as the vapour pressure on the melt surface and $f(p_i)$ stands for the functional dependence on the inner gas pressure inside the nozzle. This formulation is taken directly from Low et al. [33].

3.5. Vapourisation velocity

An expression for V_v, the normal velocity of the vapourisation front, is now developed. Two coupled expressions are used. V_v is directly related to the amount of power taken up by vapourisation. In this section an additional expression, based on the simultaneous condition, that the mass flow of vapour through the drilled hole is related to the pressure drop along the hole, is developed. The starting point is the energy balance equation for flow through a channel:

$$A\frac{v_v^2}{2} + g\Delta z + \int_{Low}^{High} \frac{dp}{\rho_v} + \widehat{F} = \widehat{w} \tag{14}$$

Each term represents energy per unit mass for the fluid. The first term on the left-hand side represents change in kinetic energy. Here v_v is the vapour velocity (not V_v, the velocity of the vapourisation front). Since the diameter of the drilled hole is taken as constant, mass flux remains constant through the length of the hole, and this term is ignored. The second term represents work done to overcome gravity, and is also ignored because of the shallowness of the hole. The third term is the pressure drop, between the channel limits, required to sustain the flow. The fourth term represents the work done against friction. On the right-hand side $\widehat{w}$ is the energy directly supplied to the fluid, e.g. by mechanical pumping. In the case of laser drilling $\widehat{w}$ is zero, since the energy is supplied indirectly by vapourisation, from the point of view of the fluid. Thus, using the Moody expression for $\widehat{F}$ [38], Eq. (14) becomes

$$\int_{Low}^{High} \frac{dp}{\rho_v} = -\widehat{F} = \frac{f_{vap} L v_v^2}{2d} \tag{15}$$

Here, f_{vap} is the friction factor, L is the channel length, d its diameter, and v_v is the velocity of the vapourised material moving upward through the channel. The friction factor is relatable to the relative surface roughness and the Reynolds number of the flow, and is either determined experimentally, or taken from literature graphs, as e.g. given by

Moody [38]. First, the vapour velocity is formulated in terms of mass flow and density by

$$\dot{m}_v = \frac{v_v \rho_v \pi d^2}{4} \tag{16}$$

An expression for v_v^2 to substitute into Eq. (15) is easily derived as follows:

$$v_v = \frac{\dot{m}_v 4}{\rho_v \pi d^2} \tag{17}$$

$$v_v^2 = \frac{\dot{m}_v^2 16}{\rho_v^2 \pi^2 d^4} \tag{18}$$

Substituting Eq. (18) into Eq. (15) one obtains

$$\int_{\text{Low}}^{\text{High}} \rho_v \, \mathrm{d}p = \frac{f_{\text{vap}} L \dot{m}_v^2 8}{\pi^2 d^5} \tag{19}$$

Since

$$\rho_v = \frac{nM_m}{V} = \frac{pM_m}{RT_s} \tag{20}$$

integration of Eq. (19) yields

$$\frac{1}{2}\left[(p_{\text{vap}} + p_{\text{eff}})^2 - p_{\text{eff}}^2\right]\frac{M_m}{RT_s} = \frac{f_{\text{vap}} L \dot{m}_v^2 8}{\pi^2 d^5} \tag{21}$$

Isolating $\dot{m}_v^2$ on the left-hand side one has

$$\dot{m}_v^2 = \frac{1}{16}\frac{\pi^2 d^5}{f_{\text{vap}} L}\left[(p_{\text{vap}} + p_{\text{eff}})^2 - p_{\text{eff}}^2\right]\frac{M_m}{RT_s} \tag{22}$$

and accepting only the positive root one obtains the expression

$$\dot{m}_v = \frac{1}{4}\frac{\pi d^{\frac{5}{2}}}{f_{\text{vap}}^{\frac{1}{2}} L^{\frac{1}{2}}}\left[(p_{\text{vap}} + p_{\text{eff}})^2 - p_{\text{eff}}^2\right]^{\frac{1}{2}}\left(\frac{M_m}{RT_s}\right)^{\frac{1}{2}} \tag{23}$$

Since

$$\dot{m}_v = \frac{\rho_m V_v \pi d^2}{4} \tag{24}$$

one can now find the required expression for V_v

$$V_v = \frac{4\dot{m}_v}{\rho_m \pi d^2} = \left(\frac{4}{\rho_m \pi d^2}\right)\left(\frac{1}{4}\frac{\pi d^{\frac{5}{2}}}{f_{\text{vap}}^{\frac{1}{2}} L^{\frac{1}{2}}}\right)\left[(p_{\text{vap}} + p_{\text{eff}})^2 - p_{\text{eff}}^2\right]^{\frac{1}{2}}\left(\frac{M_m}{RT_s}\right)^{\frac{1}{2}} \tag{25}$$

Simplification gives

$$V_v = \left(\frac{\mathrm{d}^{\frac{1}{2}}}{f_{\text{vap}}^{\frac{1}{2}} L^{\frac{1}{2}} \rho_m}\right)\left[(p_{\text{vap}} + p_{\text{eff}})^2 - p_{\text{eff}}^2\right]^{\frac{1}{2}}\left(\frac{M_m}{RT_s}\right)^{\frac{1}{2}} \tag{26}$$

and

$$V_v = \frac{1}{\rho_m}\left(\frac{M_m d}{RT_s L}\right)^{\frac{1}{2}}\left[(p_{\text{vap}} + p_{\text{eff}})^2 - p_{\text{eff}}^2\right]^{\frac{1}{2}} f_{\text{vap}}^{-\frac{1}{2}} \tag{27}$$

An expression for the friction factor now needs to be found. Over any limited Reynolds number range it has the form of a decaying exponential. Thus

$$f_{\text{vap}} = a Re^{-b} \tag{28}$$

and

$$f_{\text{vap}}^{-\frac{1}{2}} = a^{-\frac{1}{2}} Re^{\frac{b}{2}} \tag{29}$$

where a and b are empirical constants, dependent of the relative surface roughness of the channel. Since the surface roughness of the drilled hole, especially during drilling, is unknown, a and b will be used as fitting parameters and the expression for V_v derived in terms of them. The Reynolds number can be expressed in terms of mass flow by

$$Re = \frac{\rho v_v d}{\mu_v} = \frac{4\dot{m}_v}{\pi d \mu_v} \tag{30}$$

Substitution of Eqs. (30) and (24) into Eq. (29) gives

$$f_{\text{vap}}^{-\frac{1}{2}} = a^{-\frac{1}{2}}\left(\frac{\rho_m V_v d}{\mu_v}\right)^{\frac{b}{2}} \tag{31}$$

Substitution of Eq. (31) into Eq. (27) gives

$$V_v = \frac{1}{\rho_m}\left(\frac{M_m d}{RT_s L}\right)^{\frac{1}{2}}\left[(p_{\text{vap}} + p_{\text{eff}})^2 - p_{\text{eff}}^2\right]^{\frac{1}{2}} a^{-\frac{1}{2}}\left(\frac{\rho_m V_v d}{\mu_v}\right)^{\frac{b}{2}} \tag{32}$$

Eq. (32) can now be rearranged to provide a solution for V_v

$$V_v^{1-\frac{b}{2}} = \frac{1}{\rho_m}\left(\frac{M_m d}{RT_s L}\right)^{\frac{1}{2}}\left[(p_{\text{vap}} + p_{\text{eff}})^2 - p_{\text{eff}}^2\right]^{\frac{1}{2}} a^{-\frac{1}{2}}\left(\frac{\rho_m d}{\mu_v}\right)^{\frac{b}{2}} \tag{33}$$

and thus

$$V_v = \left[\frac{1}{\rho_m}\left(\frac{M_m d}{RT_s L}\right)^{\frac{1}{2}}\left[(p_{\text{vap}} + p_{\text{eff}})^2 - p_{\text{eff}}^2\right]^{\frac{1}{2}} a^{-\frac{1}{2}}\left(\frac{\rho_m d}{\mu_v}\right)^{\frac{1}{2}}\right]^{\frac{1}{1-\frac{b}{2}}} \tag{34}$$

Finally an expression for hole depth, L, needs to be found. Since the final hole depth is the product of the drilling velocity and the pulse width, we estimate an average hole depth from

$$L = \frac{1}{2} V_d \tau \tag{35}$$

V_v can now be expressed in terms of the drilling velocity, V_d, and pulse width τ

$$V_v = \left[\frac{a^{-\frac{1}{2}}}{\rho_m}\left(\frac{2M_m d}{RT_s \tau}\right)^{\frac{1}{2}}\left[(p_{\text{vap}} + p_{\text{eff}})^2 - p_{\text{eff}}^2\right]^{\frac{1}{2}}\left(\frac{\rho_m d}{\mu_v}\right)^{\frac{b}{2}}\right]^{\frac{1}{1-\frac{b}{2}}}\left(\frac{1}{V_d}\right)^{\frac{1}{2-b}} \tag{36}$$

3.6. Effect of the exothermic reaction

During laser materials processing, the assist gas jet influences the process in several ways. The gas helps to remove the molten material and protects the optics of the system by keeping away both the vapour generated and the ejected

melt. An exothermic reaction is generated when the assist gas contains O_2 and if the material is reactive, e.g. a metal. The additional heat generated at the melt surface enhances process efficiency. Since O_2 assist gas is used in most practical laser drilling processes, it is important to consider the contribution of exothermic reactions in the model.

During the drilling process, the elements within the metal or alloy can be oxidised, forming various oxide phases. In general the total chemical equation for the reaction between a metal, Me, and oxygen gas, O_2, to form an oxide Me_aO_b may be written as $a\mathrm{Me} + (b/2)\mathrm{O_2} \rightarrow \mathrm{Me}_a\mathrm{O}_b$, where a and b in this case are appropriate stoichiometric coefficients. In order to quantify the additional thermal input, the heat generated by each metal element in a given metal matrix needs to be considered separately. The rate of reaction is determined by the drilling velocity as it controls the rate at which the parent material is made available for the oxidation reaction. The reaction rate, R_{ox} (in mol s^{-1}), for any particular metal element under consideration is

$$R_{ox} = \alpha_{ox} \frac{V_d \pi r_l^2 \rho_m m_{ox}}{M_{r,ox}} \tag{37}$$

Here $M_{r,ox}$ is the relative atomic mass of the metal element in consideration and m_{ox} is the mass fraction in the solid matrix of the element under consideration, and α_{ox} is the fraction of the element actually oxidised. It should be clearly grasped that the oxygen has to get to the metal surface to react, and all the metal ejected from the drilled hole cannot be expected to react with the oxygen. The oxidation process should clearly be expected to be mass transfer limited. From Eq. (37) the heat generated due to the oxidation of a particular element can be expressed as

$$P_{r,ox} = \alpha_{ox} \left(\frac{V_d \pi r_l^2 \rho_m}{M_{r,ox}} \right) m_{ox} \Delta H_{ox} \tag{38}$$

where ΔH_{ox} is the enthalpy of oxidation to form a particular oxide. For example, a possible oxidation reaction of low carbon steel is $\mathrm{Fe} + 1/2\,\mathrm{O_2} \rightarrow \mathrm{FeO}$: $\Delta H_{ox} = -242.758$ kJ mol^{-1} [39]. The total heat generated during the oxidation of a multi-element alloy can be described as follows:

$$P_r = \sum_{i=1}^{m_0} \alpha_{ox,i} \left(\frac{V_d \pi r_l^2 \rho_m}{M_{r,ox,i}} \right) m_{ox,i} \Delta H_{ox,i} \tag{39}$$

Here one assumes that a distinct oxide is formed from each element. The formulation above is different to that of Low et al., in that the oxidation process is not assumed to go to completion. The degree of oxidation is left as a variable parameter which is to be determined experimentally.

3.7. Energy balance

The following section considers the energy balance in the molten layer exposed to the laser beam when a quasi-steady-state melt ejection from the interaction zone has been reached. The melt front is moving into the solid with average velocity V_d. The solid melts and then the melt is partially ejected in the reverse direction by the trapped vapour pressure and the assist gas pressure with velocity V_m and partially evaporated from the melt surface. The input power into the molten layer can be expressed as

$$P_{in} = I_{abs} \pi r_l^2 + P_r \tag{40}$$

where I_{abs} is the absorbed laser intensity, πr_l^2 is the area (A_l) of the incident laser beam and P_r is the reactive power generated due to oxidation when an O_2 assist gas is employed. The output power of the molten layer is comprised of a conduction term, P_{cond}, a forced convection term, P_{conv}, the power required for heating and melting, P_{melt}, as well as the power required for vapourisation, P_{vap}, and can be written as follows:

$$P_{out} = P_{conv} + P_{cond} + P_{melt} + P_{vap} \tag{41}$$

Obviously the input power is equal to the output power.

A model for forced convection perpendicular to a plate is introduced as a rough approximation. The heat transfer by forced convection between the melt surface at the hole bottom and the gas flowing perpendicularly to the melt surface is addressed. The considered area is the laser beam spot size, and the heat transfer between the hole walls and the assist gas is assumed negligible. This is a reasonable approximation since the main concern is to investigate the cooling rate of the melt surface, which directly affects the drilling velocity. Firstly, the Reynolds number for the assist gas flow can be expressed as

$$Re = \frac{\rho_g v_g 2 r_l}{\mu_g} \tag{42}$$

where ρ_g is the assist gas density, v_g is flow velocity of the assist gas, μ_g is the dynamic viscosity of the gas and the width of the melt surface is taken as the laser beam spot size $2r_l$. The convective cooling rate per unit area, q, between the impinging assist gas and the melt surface is

$$q = -h(T_s - T_i) \tag{43}$$

where T_s and T_i are the melt surface and assist gas temperatures respectively, h is the heat transfer coefficient, which can be determined from

$$h = \frac{k_g}{2 r_l} (C_c Re^{n_c} Pr^{\frac{1}{3}}) \tag{44}$$

Here k_g and Pr are the thermal conductivity and Prandtl number respectively of the assist gas, C_c and n_c are experimentally determined constants for forced convection perpendicular to the melt surface, and are taken to be 0.228 and 0.731 respectively [40]. The expression in bracket on the right-hand side of Eq. (44) is the Nusselt number. Combining Eqs. (42)–(44), the power lost due to cooling by the assist gas, P_{conv}, within the melt surface area can be written as

$$P_{conv} = \frac{C_c k_g}{2 r_l} \left(\frac{\rho_g v_g 2 r_l}{\mu_g} \right)^{n_c} Pr^{\frac{1}{3}} (T_s - T_i)(\pi r_l^2) \tag{45}$$

It is important to mention that due to the complexity in the evaporation of surfaces, the above forced convection cooling analysis should only be regarded as a first approximation. For example, if substantial evaporation is achieved a Knudsen layer may exist and the cooling effect may be affected. Nevertheless, this is not an issue for concern as the computed results below show that power losses due to convective cooling to be minimal relative to other effects. This formulation of forced convection is standard and was also used by Low et al.

The approach to conduction losses presented here is similar to that of both Semak and Matsunawa, and Low et al. The conduction term can be estimated from the sum of forward and radial components:

$$P_{\text{cond}} \approx -k_{\text{s}}\nabla_{\text{forward}}T\pi r_{\text{l}}^2 - k_{\text{s}}\nabla_{\text{radial}}T\pi r_{\text{l}}^2 \tag{46}$$

where k_{s} is the thermal conductivity of the solid metal and the gradients of temperature are taken at the melt front along (forward) and perpendicularly (radial) to the motion of the retreating solid metal. The forward component can be written as

$$-k_{\text{s}}\nabla_{\text{forward}}T\pi r_{\text{l}}^2 = k_{\text{s}}\frac{T_{\text{m}}-T_0}{\kappa_{\text{s}}/V_{\text{d}}}\pi r_{\text{l}}^2 = \rho_{\text{s}}C_{p,\text{s}}(T_{\text{m}}-T_0)V_{\text{d}}\pi r_{\text{l}}^2 \tag{47}$$

here, κ_{s} is the thermal diffusivity of the solid metal. The radial component can be estimated from

$$-k_{\text{s}}\nabla_{\text{radial}}T\pi r_{\text{l}}^2 \approx k_{\text{s}}\frac{(T_{\text{m}}-T_0)\pi r_{\text{l}}^2}{\left[\frac{\kappa_{\text{s}}}{V_{\text{d}}}\left(r_{\text{l}}+\frac{\kappa_{\text{m}}}{V_{\text{d}}}\right)\right]^{\frac{1}{2}}} \approx \frac{\rho_{\text{s}}C_{p,\text{s}}(T_{\text{m}}-T_0)V_{\text{d}}\pi r_{\text{l}}^2}{\left(\frac{\kappa_{\text{m}}}{\kappa_{\text{s}}}+\frac{V_{\text{d}}}{\kappa_{\text{s}}}r_{\text{l}}\right)^{\frac{1}{2}}} \tag{48}$$

Since the forward component is used to pre-heat the solid metal, only the radial component is considered to be energy lost from the melt layer.

The power spent on heating and melting can be expressed as follows:

$$\begin{aligned}P_{\text{melt}} &\approx 2\pi r_{\text{l}}\rho_{\text{m}}[C_{p,\text{m}}(T^*-T_{\text{m}}) + C_{p,\text{s}}(T_{\text{m}}-T_0) + L_{\text{m}}]V_{\text{m}}\delta_{\text{m}} \\ &= 2\pi r_{\text{l}}\rho_{\text{m}}[C_{p,\text{m}}(T^*-T_{\text{m}}) + C_{p,\text{s}}(T_{\text{m}}-T_0) + L_{\text{m}}]\frac{V_{\text{m}}\kappa_{\text{m}}}{V_{\text{d}}}\end{aligned} \tag{49}$$

where T^* is the average temperature within the melt layer and is approximated by

$$T^* = T_{\text{m}} + \alpha_{\text{c}}(T_{\text{s}}-T_{\text{m}}) \tag{50}$$

T_{m} is the melting point of the solid metal and α_{c} is a constant smaller than unity. It is taken to be 0.5 in this work. Taking into account the vapourisation front velocity, V_{v}, the power used for vapourisation is given as

$$P_{\text{vap}} = \rho_{\text{m}}V_{\text{v}}L_{\text{v}}\pi r_{\text{l}}^2 \tag{51}$$

where L_{v} is the latent heat of vapourisation.

Combination of Eqs. (39)–(41), (45)–(49), (51), and division by πr_{l}^2 gives

$$\begin{aligned}I_{\text{abs}} = &-\sum_{i=1}^{m_0}\alpha_{\text{ox},i}\left(\frac{V_{\text{d}}\rho_{\text{m}}}{M_{\text{r,ox},i}}\right)m_{\text{ox},i}\,\Delta H_{\text{ox},i} \\ &+\frac{C_{\text{c}}k_{\text{g}}}{2r_{\text{l}}}\left(\frac{\rho_{\text{g}}v_{\text{g}}2r_{\text{l}}}{\mu_{\text{g}}}\right)^{n_{\text{c}}}Pr^{\frac{1}{3}}(T_{\text{s}}-T_{\text{i}}) + \rho_{\text{s}}C_{p,\text{s}}(T_{\text{m}}-T_0)V_{\text{d}} \\ &+\frac{\rho_{\text{s}}C_{p,\text{s}}(T_{\text{m}}-T_0)V_{\text{d}}}{\left(\frac{\kappa_{\text{m}}}{\kappa_{\text{s}}}+\frac{V_{\text{d}}}{\kappa_{\text{s}}}r_{\text{l}}\right)^{\frac{1}{2}}} + 2\rho_{\text{m}}[C_{p,\text{m}}(T^*-T_{\text{m}}) \\ &+C_{p,\text{s}}(T_{\text{m}}-T_0) + L_{\text{m}}]\frac{V_{\text{m}}\kappa_{\text{m}}}{V_{\text{d}}r_{\text{l}}} + \rho_{\text{m}}V_{\text{v}}L_{\text{v}}\end{aligned} \tag{52}$$

4. Physical properties

The physical properties of the solid used for drilling and the assist gas are tabulated in Tables 1 and 2.

5. Calculation procedure

The mathematical developments given in the paragraphs above constitute a system of mostly non-linear equations, the simultaneous solution of which yields relationships amongst the various system parameters and were solved using Mathcad. The approach taken to obtain solutions is as follows:

Table 1
Thermophysical properties of low carbon steel [23]

Material property	Low carbon steel
Density of solid, ρ_{s} (kg m^{-3})	7800
Density of melt, ρ_{m} (kg m^{-3})	6980
Specific heat of solid, $C_{p,\text{s}}$ (J kg^{-1} K^{-1})	628
Specific heat of liquid, $C_{p,\text{m}}$ (J kg^{-1} K^{-1})	748
Thermal diffusivity of solid, κ_{s} (m^2 s^{-1})	0.014×10^{-3}
Thermal diffusivity of melt, κ_{m} (m^2 s^{-1})	0.007×10^{-3}
Latent heat of melt, L_{m} (J kg^{-1})	276×10^3
Latent heat of vaporisation, L_{v} (J kg^{-1})	6088×10^3
Initial temperature, T_0 (K)	300
Melting point, T_{m} (K)	1808
Boiling point, T_{vap} (K)	3100
Molar mass, M_{m} (kg mol^{-1})	0.05575
Laser beam radius, r_{l} (m)	0.26×10^{-3}

Table 2
Thermophysical properties of O_2 assist gas and gas nozzle parameters [51–53]

O_2 assist gas property	Value
Nozzle pressure, p_{i} (N m^{-2})	3×10^5
Gas flow rate, f_{g} (l min^{-1}) {m^3 s^{-1}}	40 {0.667×10^{-3}}
Gas flow velocity, v_{g} (m s^{-1})	377
Density of gas, ρ_{g} (kg m^{-3})	1.3007
Viscosity of gas, μ_{g} (N s m^{-2})	2.01×10^{-5}
Prandtl number, Pr	0.73
Thermal conductivity, k_{g} (W m^{-1} K^{-1})	0.0259
Temperature of assist gas, T_{i} (K)	300
Nozzle exit diameter, d_{n} (m)	1.5×10^{-3}
Laser beam radius, r_{l} (m)	2.6×10^{-4}
Nozzle–workpiece distance, z_{n} (m)	2.2×10^{-3}

1. Assume a vapour pressure.
2. Calculate the corresponding surface temperature from the Clausius–Clapeyron equation, Eq. (9).
3. Calculate the pressure exerted by the assist gas from Eqs. (10) and (13).
4. Calculate the melt ejection velocity from Eq. (8).
5. Calculate the drilling velocity by solving for V_d in Eq. (4) after inserting the calculated value of the melt ejection velocity, and substituting Eq. (36) for V_v.
6. Then calculate the vapourisation velocity, V_v, from Eq. (36).
7. Obtain the power lost to forced convection from Eq. (45).
8. Calculate the power required for heating and phase change from Eqs. (49) and (51).
9. Get the power added to the system by the exothermic oxidation reaction from Eq. (39).
10. Calculate the forward and radial conduction power losses from Eqs. (47) and (48) respectively.
11. And finally calculate the laser intensity to sustain the process from Eq. (52).

6. Experimental procedures for model verification

The experimental results from Low et al. on drilling velocity and melt ejection velocity measurement are used for model verification [33], and a brief description is provided.

6.1. Drilling velocity measurement

A fibre-optic delivered Nd:YAG laser emitting at 1.06 μm wavelength was used in the experiments. The laser beam was focussed with a lens having a focal length of 120 mm, giving a spot size of approximately 520 μm diameter. Low carbon steel plates were drilled with actual peak powers ranging between 0.7 and 5 kW at three different pulse widths of 0.5, 1.0, and 1.5 ms. Experiments were performed with and without O_2 assist gas. None-through holes were produced so the drilling velocity can be determined by cross-sectioning of laser-drilled holes. Precision fine cutter (Struers Accutom-5) was used to section the workpiece at 0.5 mm from the edges of the holes. The sectioned holes were then mounted in polymer resin and ground with SiC emery paper until the edge of the holes were reached. This was followed by grinding with finer SiC paper until the centre of the holes was reached.

6.2. Melt ejection velocity measurement

In order to estimate the melt ejection velocity, a Kodak HS 4540 high-speed imaging system was employed to record the single-pulse drilling experiments at 9000 frames s^{-1}. The melt ejection velocity was estimated by measuring the distance travelled by the particles between two frames and dividing it by the frame period. The final melt ejection velocity was taken from the average velocity of three particles during the impingement of the laser beam.

6.3. Degree of oxidation measurement

Low carbon steel was drilled with 7 kW peak power, 0.3 ms pulse width, with O_2 assist gas at 3 bar. A glass slide was placed 40 mm below the workpiece to capture the melt ejection material. The glass slide was then mounted in polymer resin, ground with fine SiC emery paper to approximately the centre of the melt droplets. This was then followed by polishing with 3 μm diamond paste. SEM imaging and EDX analysis were performed for 10 randomly selected droplets. The percentage volume oxidation was calculated by measuring the percentage area of oxidation using image analysis software and the SEM images obtained.

7. Results and discussion

The following sections present and discuss the results obtained for the melt surface temperature, drilling velocity, and melt ejection velocity, for drilling with and without O_2 assist gas. In order to test the validity of the model, the results of the current model are compared with those calculated using the model of Low et al. and their experimental results. In addition, the investigation on the degree of oxidation that determines the value of oxidation enthalpy used in the model is discussed.

7.1. Melt surface temperature

Fig. 2 shows the predicted melt surface temperature as a function of absorbed laser intensity for drilling with and without O_2 assist gas. A general increase of melt surface temperature with absorbed laser intensity can be noted. Those drilled with O_2 show higher melt surface temperature as a result of additional energy put into the system through exothermic reaction. This was true for both Low et al.'s model and the current model. It should be noted that the model presented in this work predicts surface temperatures substantially lower than those predicted by Semak and Matsunawa [23], and Low et al. [33].

There is an increase in boiling point due to pressure build-up at the melt surface. The relationship between boiling point and vapour pressure is governed by the Clausius–Clapeyron equation, built into this model. Unlike previous models, the vapour pressure at the surface is coupled to the mass flow of the vapour through the drilled hole, thus providing a mechanism for pressure relief, and pressure cannot build-up indefinitely. Because of this, the increase in boiling point, and hence surface temperature is substantially lower than previous models.

At present, there exists no experimental data pertaining to the surface temperature inside a laser-drilled hole. It is thus difficult to come to an unambiguous decision as to which temperature prediction is correct. Nevertheless, the lower temperature seems more physical as from about

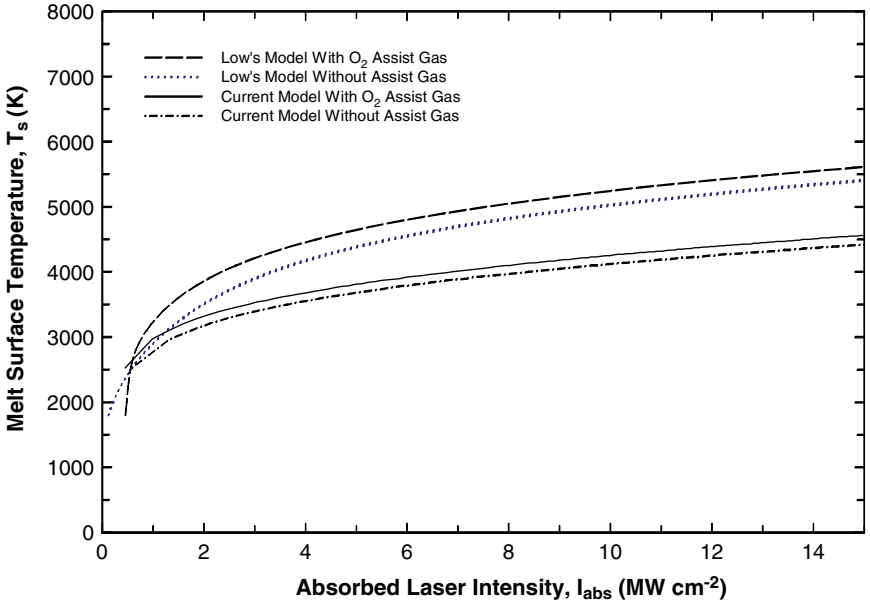

Fig. 2. Comparison of calculated relationships between temperature and absorbed laser intensity for drilling on low carbon steel with and without O_2 assist gas.

5000 K ionisation should be expected, making any further temperature increase extremely difficult, since the energy would be consumed by the ionisation process rather than by providing additional kinetic energy to the atoms.

7.2. Drilling velocity

Previous models inverted Eq. (4) to the form

$$V_d = \frac{\rho_m}{\rho_s} V_v + \frac{2\delta_m \rho_m}{r_l} V_m \tag{53}$$

in order to express V_d in its components

$$V_{dv} = \frac{\rho_m}{\rho_s} V_v \tag{54}$$

and

$$V_{dm} = \frac{2\delta_m \rho_m}{r_l} V_m \tag{55}$$

Figs. 3 and 4 contain predicted values for these quantities, using both the current model and Low et al.'s model. The variation of drilling velocity, V_d, and its corresponding

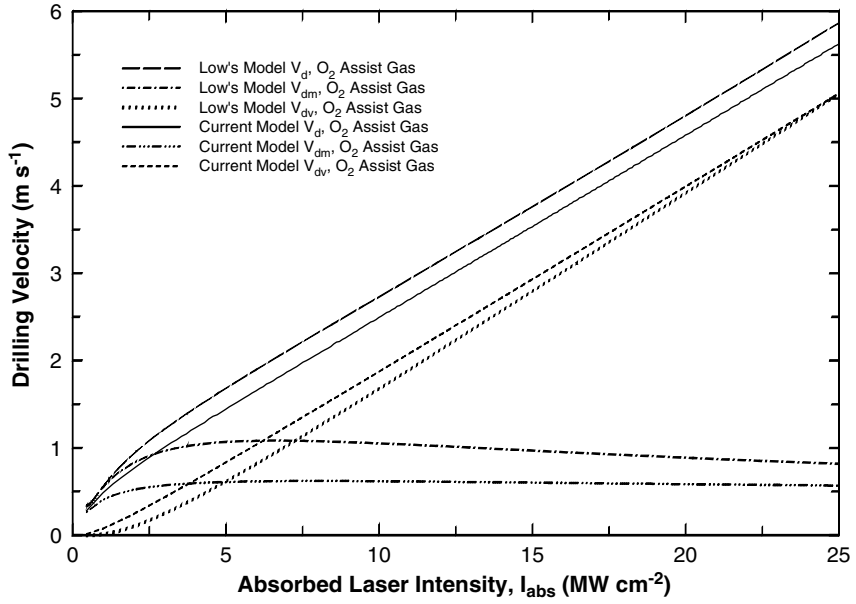

Fig. 3. Relationship between drilling velocity, V_d, and its components, V_{dm} and V_{dv}, and absorbed laser intensity for O_2 assist gas drilling on low carbon steel.

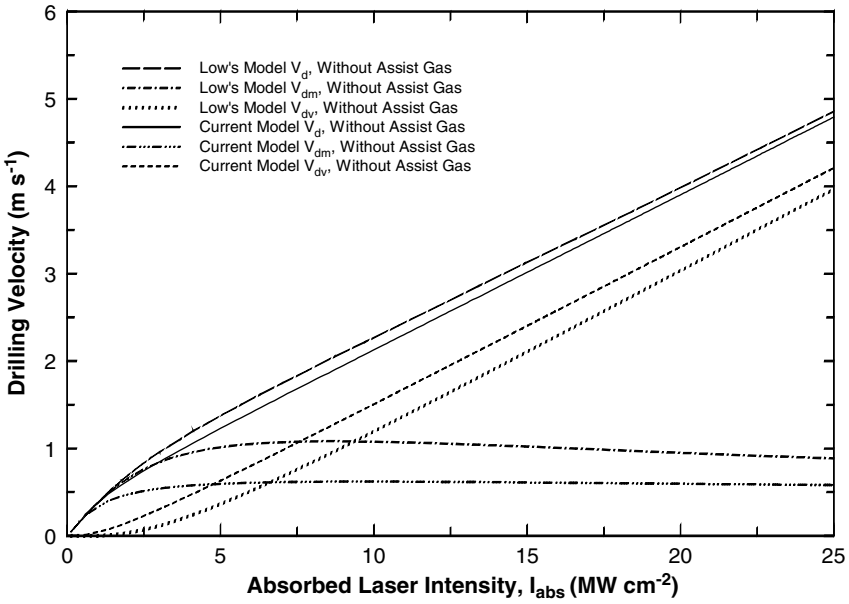

Fig. 4. Relationship between drilling velocity, V_d, and its components, V_{dm} and V_{dv}, and absorbed laser intensity for drilling without assist gas on low carbon steel.

components due to melt ejection, V_{dm}, and melt vapourisation, V_{dv}, with absorbed laser intensity; are shown for both with and without O_2 assist gas respectively. The result of the current model shows similar trend to those from Low et al. It should be noted that Low et al.'s model was reprogrammed to reproduce his results. Because the exact values of some of the coefficients used were not known (e.g. the value of V_0), therefore, the exact results are not reproduced. However, the trends and general features of the curves correspond well.

Our practical experience suggests that liquid ejection from the drilled hole contributes significantly to the total mass removed. This effect is confirmed in the literature by e.g. Voisey et al. who quantified the vapour-to-melt ratio [41]. This is confirmed by Fig. 3 which shows that at low absorbed laser intensities (below 3.8 MW cm^{-2}), the drilling velocity due to melt ejection, V_{dm}, dominates the process. Beyond 3.8 MW cm^{-2}, the drilling velocity due to vapourisation, V_{dv}, becomes the dominant component. However, it should be noted that such absorbed laser

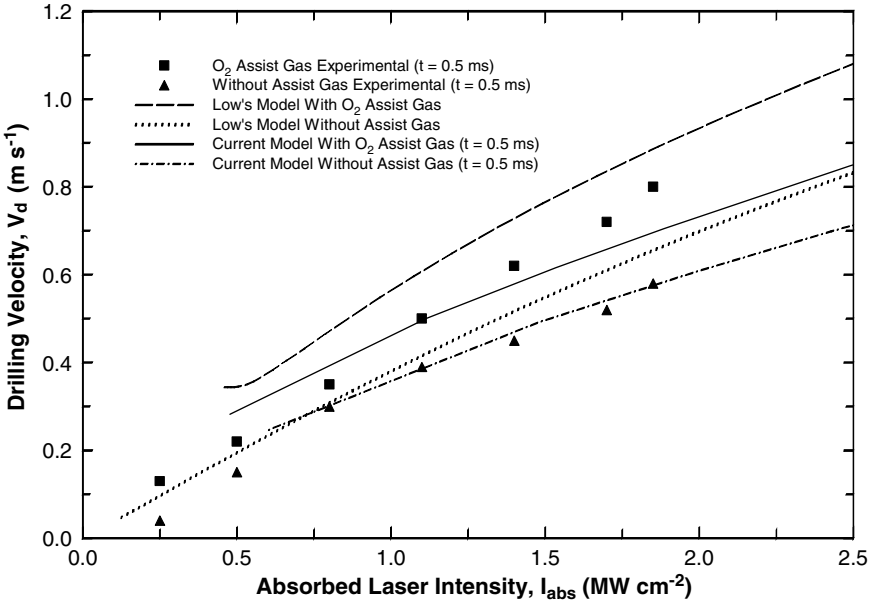

Fig. 5. Comparison between the predicted and experimental drilling velocities for drilling on low carbon steel with and without O_2 assist gas using 0.5 ms laser pulse width.

intensity far exceeds the capability of the laser system used in this experiment (~3 MW cm^{-2}). Similarly, the threshold value at which the vapourisation component becomes dominant when laser drilling without assist gas is approximately 4.8 MW cm^{-2}. The main difference between the model presented here, and Low et al.'s, is that the onset of the vapourisation-dominated regime is predicted to be earlier. This is due to the fact that pressure relief is built into the current model. From these predicted results, it could also be deduced that the maximum drilling velocity at 1.0 ms pulse width, is approximately 1 m s^{-1} when drilling with O_2 assist gas, and 0.8 m s^{-1} when drilling without assist gas.

Figs. 5–7 show the comparison between the predicted model and experimentally measured results for drilling velocity with and without O_2 assist gas, using single pulse with pulse widths of 0.5, 1.0, and 1.5 ms respectively. Low et al.'s model over-predicts the drilling velocities in all cases. Not only that, the model addresses steady-state conditions and therefore does not account for pulse widths. Hence, Low et al.'s results given in Figs. 5–7 are identical. Whereas the model presented here does take pulse width

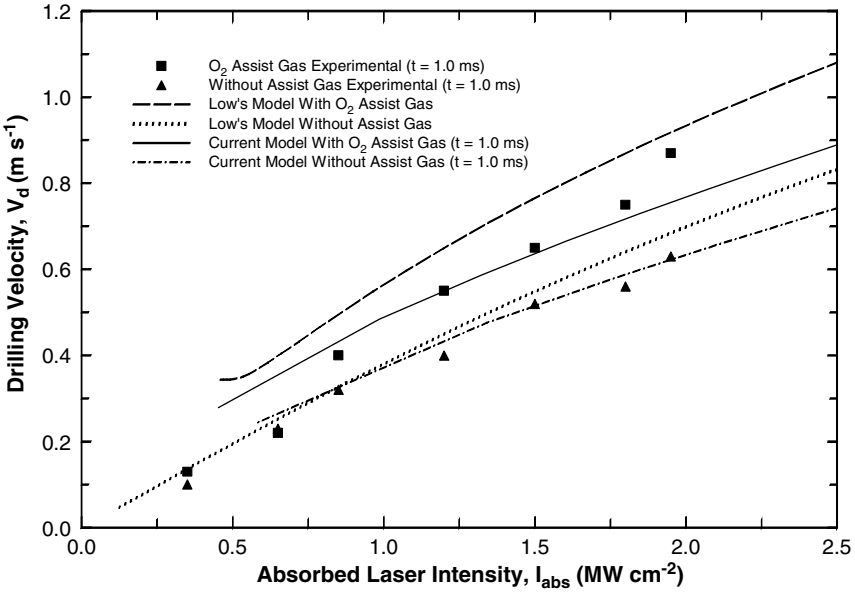

Fig. 6. Comparison between the predicted and experimental drilling velocities for drilling on low carbon steel with and without O_2 assist gas using 1.0 ms laser pulse width.

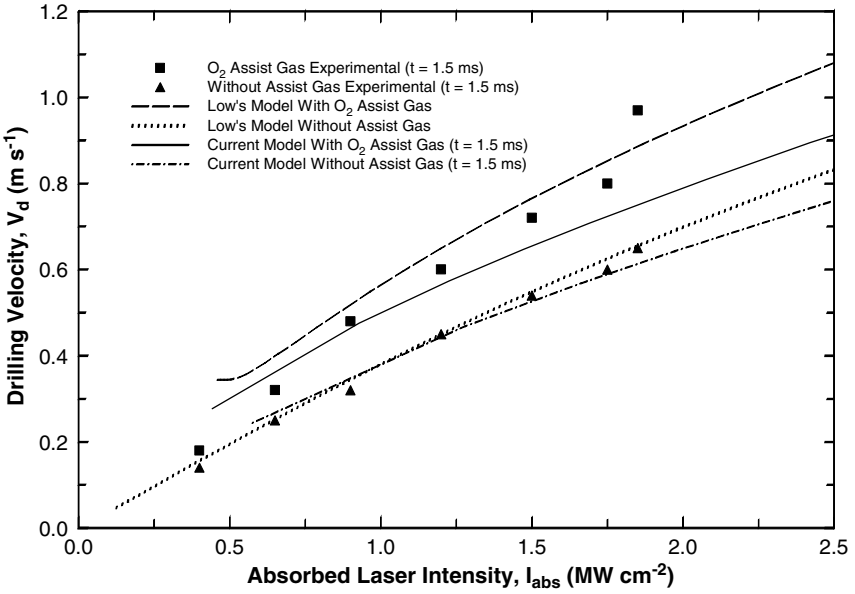

Fig. 7. Comparison between the predicted and experimental drilling velocities for drilling on low carbon steel with and without O_2 assist gas using 1.5 ms laser pulse width.

into account via the hole depth. The deeper the hole, the greater is the pressure build-up and, the greater will be the melt ejection velocity and the drilling velocity. For all three pulse width cases given in Figs. 5–7, excellent fits are obtained. There does appear to be a consistent upturn in the experimentally measured drilling velocities with oxygen at high-laser intensities. This could possible not be an artefact, but rather a non-linear effect not accounted for by the model. Curve fitting was done by adjustment of the two parameters for the exponentially decaying friction factor. These values were held constant for all curves presented here. The values for a and b thus obtained correspond to a rather high relative surface roughness. This is acceptable since one would expect high flow resistance due to the fact that two-phase flow takes place in the drilled hole during the drilling process. It should be

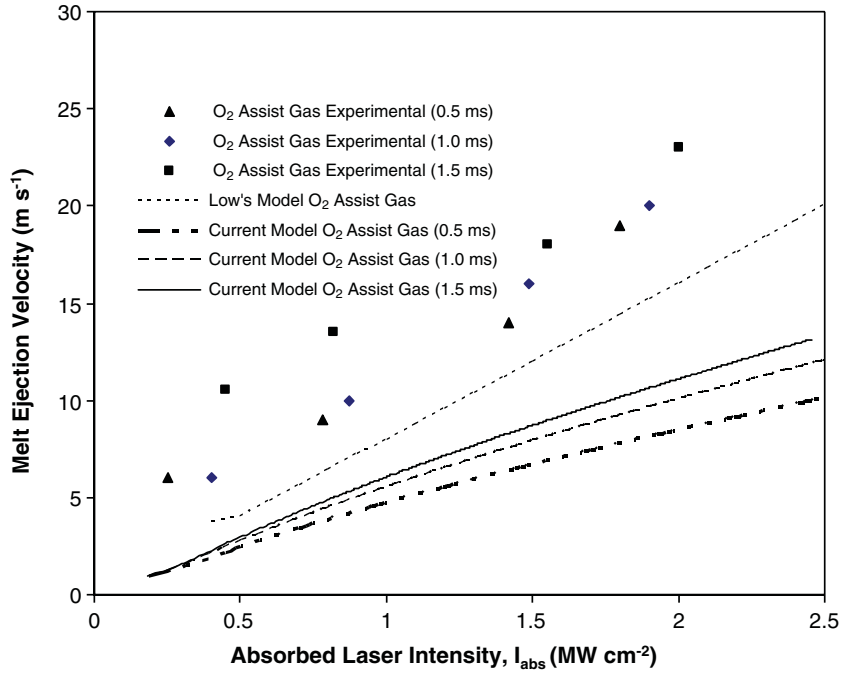

Fig. 8. Comparison between the predicted and experimental melt ejection velocities for drilling on low carbon steel with O_2 assist gas for 0.5 ms, 1.0 ms and 1.5 ms pulse widths.

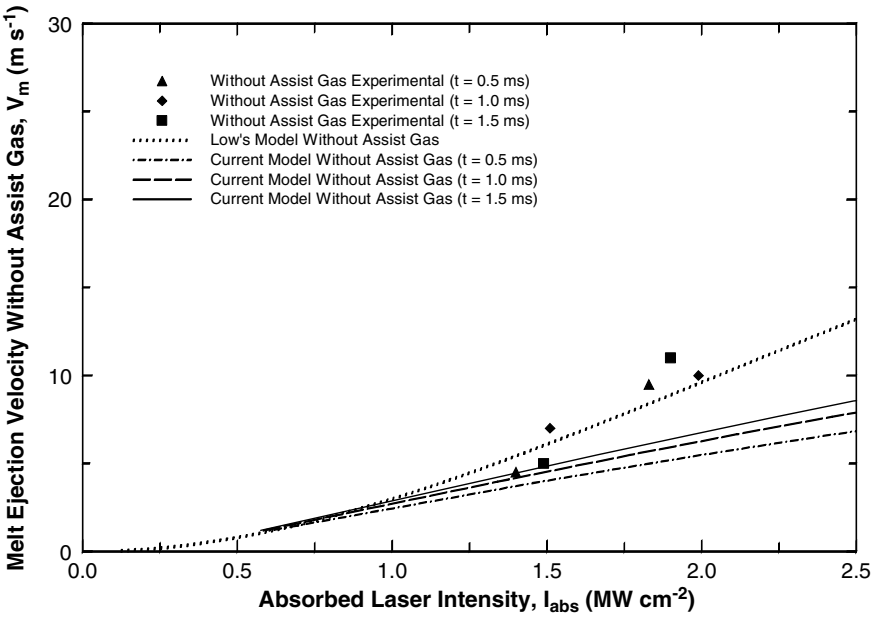

Fig. 9. Comparison between the predicted and experimental melt ejection velocities for drilling on low carbon steel without assist gas for 0.5 ms, 1.0 ms and 1.5 ms pulse widths.

mentioned that Low et al.'s model data proved somewhat difficult to reproduce since the exact value for V_0 was not stated.

7.3. Melt ejection velocity

Figs. 8 and 9 show the comparison between the predicted model and experimentally measured melt ejection velocities for drilling with and without O_2 assist gas respectively, using 0.5, 1.0, and 1.5 ms laser pulse widths. Whilst Low et al.'s model does not make the distinction between different laser pulse widths, the current model correctly predicts the observed trends; that is, the longer the pulse width, the higher the melt ejection velocity.

Both predicted results and experimental results show higher melt ejection velocities when O_2 gas is used, the

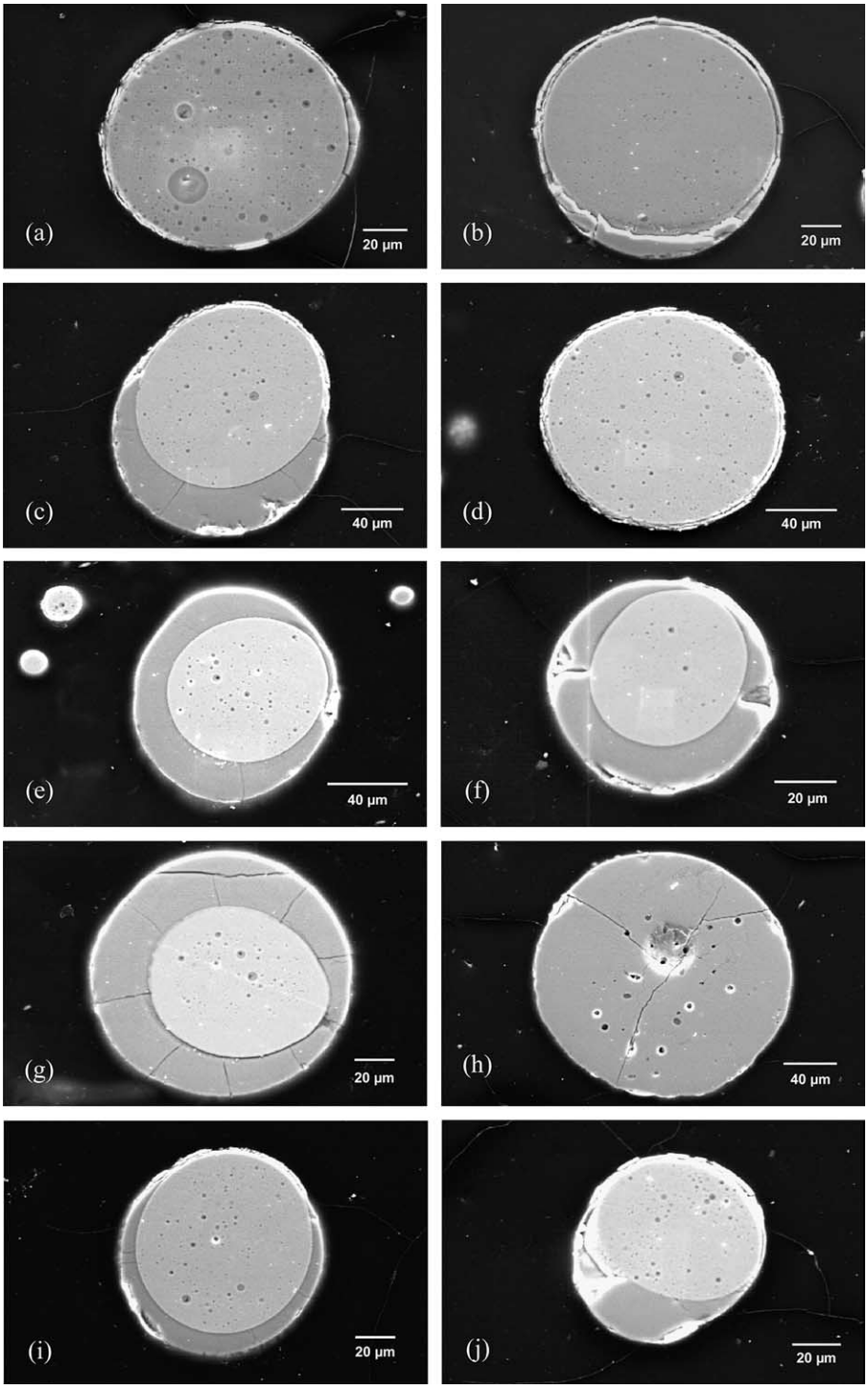

Fig. 10. Typical SEM micrographs of cross-sectioned melt droplets.

result of the additional energy from the exothermic reaction of the assist gas. This leads to an increase in the recoil pressure and hence more efficient melt ejection. In drilling with and without O_2 assist gas, Low et al.'s model obtained better agreements with the experimental results, albeit under-predicting the melt ejection velocity when O_2 gas is used. It should be mentioned that despite the use of high-speed imaging system, the method of measurement has an error of ±30% due to the difficulty in the determination of the direction of melt ejection [42]. Not only that, the high-speed imaging method is biased towards higher velocities because the melt ejection beyond the end of the pulse is not observed. Late ejected, slow moving droplets may therefore either completely miss being recorded or will have moved too small a fraction of the field of view to be observed. It should also be borne in mind that there exist two general mechanisms of melt ejection. A possible mechanism of material removal is the recoil-pressure driven flow of molten material that travels along the walls of the hole, followed by break up into droplets upon exiting the hole. Alternatively, explosions due to nucleate boiling could expel the material to form molten droplets [43]. If this mechanism does in fact exists, then it is possible that the ejected particles studied by the use of high-speed imaging system had followed such particles rather than the slower particles induced by the recoil pressure. Hence the measured ejection velocity will not correspond to the velocity predicted by the model based on recoil pressure. Not only that, the melt ejection process is stochastic and there exists a particle size distribution. The ejection velocity of the individual melt droplet is directly related to the particle size, with larger droplets travelling at lower velocities and smaller droplets traversing at higher velocities. An additional unknown, not addressed by the model, is the effect of the physical properties of the oxide film on the droplet trajectory and velocity. To complicate matters further, there is published evidence [44] that the assist gas has a decelerating effect on the ejected droplets. To account for this an additional decelaration term would have to be added to Eq. (7). The comparison with experimental drilling velocity data is hence not entirely a clear indication of model validity. Despite large deviation between predicted results and experimental results, the model predicts a melt ejection velocity of up to 13.1 m s^{-1}, and up to 8.5 m s^{-1} for drilling with and without O_2 assist gas respectively, which nevertheless, corresponds well with published values of 1–30 m s^{-1} [42,45,46].

7.4. Effect of oxidation

The enthalpy of oxidation used in Low et al.'s model which referenced Barin and Knacke [47] refers to iron monoxide and was −158.75 kJ mol^{-1} (at 1800 K). However, this value appears to be erroneous. For this work the oxidation product was assumed to be Fe_2O_3 (as discussed below), and the value of enthalpy of oxidation (per mole *oxide*) used was taken to be −826.72 kJ mol^{-1} [39,48,49]. Since not all the ejected material will be oxidised, α_{ox} is introduced to take into account of the percentage of oxidation. This percentage was deduced experimentally. Fig. 10 shows the cross-section of a number of captured molten droplets, revealing the percentage area of oxidised material, which is found to vary substantially from one droplet to another. In general, the metal portion of the droplets are encapsulated by a varying degree of oxidised material, and in most cases, oxidised material are also distributed within the metal. The oxidised material, which appears darker than the metal under SEM were verified by energy

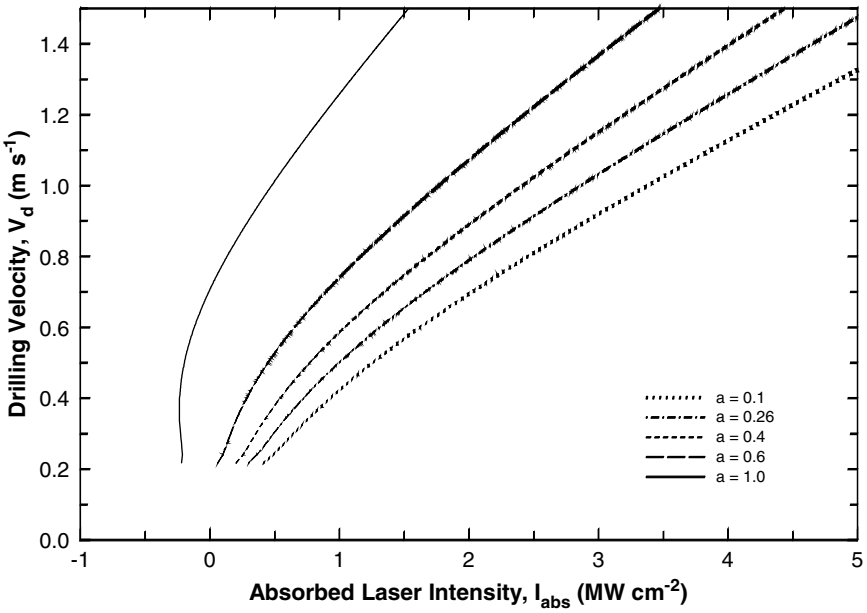

Fig. 11. The effect of degree of oxidation on the predicted relationship between drilling velocity and laser intensity.

dispersive X-ray (EDX) analysis and shows to possess approximately 60% atomic percentage of oxygen. This suggests that the oxidised material is in fact haematite, Fe_2O_3. The oxidised material is characterised by cracks that runs from the surface towards the inside of the droplet and cease upon reaching the metal substrate.

The percentage oxidation was found to be $26 \pm 18\%$. This was the value used to generate the model data. Modelling results presented in Fig. 11 show the huge impact the degree of oxidation has on the power requirement. If 100% oxidation is assumed, the contribution of the oxidation reaction to the process is such that it completely dominates. In fact, negative laser power requirement are predicted. This is obviously non-sensical and one can conclude that in theory not all the ejected material can be oxidised. Of course, if it were oxidised in flight, then the reaction enthalpy would serve to erode the wall rather than contribute to the drilling speed.

8. Conclusions

A one-dimensional analytical model previously developed by Semak and Matsunawa [23], and adapted for the laser drilling process by Low et al. [33], has been modified to include the effects of pulse width variation, and the formulation of recoil pressure can take into account hole depth and brings pressure variation into the model. The fraction of enthalpy of oxidation was determined experimentally. The model developed was based on the realistic material removal mechanisms of vapourisation and melt ejection for laser beam intensities used in this experiment.

The model identifies that the power lost due to the cooling effect of the O_2 assist gas was negligible, which agrees with the finding of Duley and Gonsalves [3], and Kamalu and Steen [50]. Instead, the O_2 assist gas provides additional energy to the system and results in higher melt surface temperatures. In close agreement with the experimental results, the analytical model predicts an increase in drilling velocity and melt ejection velocities when O_2 assist gas is used. It was also deduced from the model that the percentage of oxidation has significant influence on the drilling velocity and shows a marked increase in drilling velocity with increase in the oxidised fraction.

References

[1] J.F. Ready, Effects due to absorption of laser radiation, J. Appl. Phys. 36 (2) (1965) 462–468.

[2] U.C. Paek, F.P. Gagliano, Thermal analysis of laser drilling process, IEEE J. Quant. Electron. QE8 (1972) 112–119.

[3] W.W. Duley, J.N. Gonsalves, Interaction of CO_2 laser radiation with solids. Drilling of fused quartz, Can. J. Phys. 50 (1972) 216–221.

[4] C. Bar-Isaac, U. Korn, Moving heat source dynamics in laser drilling processes, Appl. Phys. 3 (1974) 45–54.

[5] J.G. Andrews, D.R. Atthey, On the motion of an intensely heated evaporating boundary, J. Inst. Math. Appl. 15 (1975) 59–72.

[6] M. Von Allmen, Laser drilling velocity in metals, J. Appl. Phys. 47 (1976) 5460–5463.

[7] R.E. Wagner, Laser drilling mechanics, J. Appl. Phys. 45 (1974) 4631–4637.

[8] E. Armon, G. Laufer, The response of living tissue to pulses of a surgical CO_2 laser, Trans. ASME: J. Biomech. Eng. 107 (1985) 286–290.

[9] E. Armon, G. Laufer, Asymptotic and dimensionless analysis of the responses of living tissue to surgical pulsed CO_2 lasers, Trans. ASME: J. Biomech. Eng. 108 (1986) 369–371.

[10] C.L. Chan, J. Mazumder, One-dimensional steady-state model for damage by vaporisation and liquid expulsion due to laser-material expulsion, J. Appl. Phys. 62 (1987) 4579–4586.

[11] A. Kar, J. Mazumder, Two-dimensional model for material damage due to melting and vaporisation during laser irradiation, J. Appl. Phys. 68 (1990) 3884–3891.

[12] E. Armon, Y. Zvirin, A. Solan, Numerical-simulation of metal drilling with a CO_2 laser beam, Numer. Heat Transfer, Part B: Fundamentals 19 (1991) 85–104.

[13] J.O. Vorreiter, D.A. Kaminski, R.N. Smith, Monte-Carlo simulation of a laser drilling process, Proc. ASME 91 (WA-HT-9) (1991) 1–7.

[14] R.S. Patel, M.Q. Brewster, Gas-assisted laser metal drilling: theoretical model, J. Thermophys. Heat Transfer 5 (1991) 32–39.

[15] M. He, P.J. Bishop, A. Minardi, Prediction of cavity shape and material removal rates using a two dimensional axisymmetric heat conduction model for fibrous ceramic insulation and comparison with experiments, J. Laser Appl. 5 (1993) 33–40.

[16] A. Kar, T. Rockstroh, T.J. Mazumder, Two-dimensional model for laser-induced materials damage: effects of assist gas and multiple reflections inside the cavity, J. Appl. Phys. 71 (1992) 2560–2569.

[17] A. Kar, J. Mazumder, Mathematical model for multiple reflections during laser drilling, in: Proceedings of ICALEO'94, Orlando, FL, 1994, pp. 490–498.

[18] C.D. Boley, Computational model of drilling with high radiance pulsed lasers, in: Proceedings of ICALEO'94, Orlando, FL, 1994, pp. 499–508.

[19] R.K. Ganesh, W.W. Bowley, R.R. Bellantone, Y. Hahn, A model for laser hole drilling in metals, J. Comput. Phys. 125 (1996) 161–176.

[20] T.M. Yue, C.Y. Jiang, J.H. Xu, W.S. Lau, Laser fantasy: from machining to welding, J. Mater. Process. Technol. 57 (1996) 316–319.

[21] R.K. Ganesh, A. Faghri, Y. Hahn, A generalized thermal modeling for laser drilling process—I. Mathematical modeling and numerical methodology, Int. J. Heat Mass Transfer 40 (1997) 3351–3360.

[22] R.K. Ganesh, A. Faghri, Y. Hahn, A generalized thermal modeling for laser drilling process—II. Numerical simulation and results, Int. J. Heat Mass Transfer 40 (1997) 3361–3373.

[23] V. Semak, A. Matsunawa, The role of recoil pressure in energy balance during laser materials processing, J. Phys. D: Appl. Phys. 30 (1997) 2541–2552.

[24] V. Semak, X. Chen, K. Mundra, J. Zhao, Numerical simulation of hole profile in high beam intensity laser drilling, in: Proceedings of ICALEO'97, San Diego, CA, 1997, pp. 81–89.

[25] J.J. Batteh, M.M. Chen, J. Mazumder, Scaling and numerical analysis of pulse laser drilling, in: Proceedings of ICALEO'98, Orlando, FL, 1998, pp. 30–39.

[26] C.L. Chan, Transient 1-D laser drilling model with variable properties, in: Proceedings of ICALEO'99, San Diego, CA, 1999, pp. 21–30.

[27] Y. Zhang, A. Faghri, Vaporisation, melting and heat conduction in the laser drilling process, Int. J. Heat Mass Transfer 42 (1999) 1775–1790.

[28] P. Solana, P. Kapadia, J.M. Dowden, P.J. Marsden, An analytical model for the laser drilling of metal with absorption within the vapour, J. Phys. D: Appl. Phys. 32 (1999) 942–952.

[29] J.J. Batteh, M.M. Chen, J. Mazumder, Integral analysis of the heat and momentum transfer in laser drilling, in: Proceedings of ICALEO'99, San Diego, CA, 1999, pp. 31–40.

[30] J. Cheng, F.J. Kahlen, A. Kar, Effects of intra-pulse structure on hole geometry in laser drilling, J. Laser Appl. 12 (6) (2000) 232–238.

[31] C.L. Chan, D.W. Campbell, R.D. Rosenwald, A.E. Paul, The threshold and efficiency of material removal, in: Proceedings of ICALEO'00, Detroit, MI, 2000, pp. 246–255.
[32] S.D. Silva, C.L. Chan, Coupled boundary element method and finite difference method for laser drilling, in: Proceedings of ICALEO'00, Detroit, MI, 2000, pp. 193–201.
[33] D.K.Y. Low, L. Li, P.J. Byrd, Hydrodynamic physical modelling of laser drilling, J. Manufact. Sci. Eng. 124 (2002) 852–862.
[34] J. Frenkel, Kinetic Theory of Liquids, Oxford University Press, London, 1946.
[35] D.A. McQuarrie, J.D. Simon, Physical Chemistry—A Molecular Approach, University Science Books, Sausalito, 1997.
[36] P.W. Atkins, Physical Chemistry, seventh ed., Oxford University Press, Oxford, 2002.
[37] A.F.H. Kaplan, An analytical model of metal cutting with a laser beam, J. Appl. Phys. 79 (1996) 2198–2208.
[38] L.F. Moody, Trans. ASME 66 (1944) 671–684.
[39] I. Barin, Thermochemical Data of Pure Substances, third ed., VCH, WeinHeim and New York, 1995.
[40] M. Jakob, Heat Transfer, John Wiley, New York, 1959.
[41] K.T. Voisey, C.F. Cheng, T.W. Clyne, Quantification of Melt Ejection Phenomena during Laser Drilling, Met. Res. Soc. Symp., vol. 617, 2000.
[42] W.S.O. Rodden, P. Solana, S.S. Kudesia, D.P. Hand, P. Kapadia, J. Dowden, J.D.C. Jones, Melt-ejection processes in single pulse Nd:YAG laser drilling, in: Proceedings of ICALEO'99, San Diego, CA, 1999, pp. 61–69.
[43] B.S. Yilbas, M. Sami, Liquid ejection and possible nucleate boiling mechanisms in relation to the laser drilling process, J. Phys. D: Appl. Phys. 30 (1997) 1996–2005.
[44] W.S.O. Rodden, S.S. Kudesia, D.P. Hand, J.D.C. Jones, Use of 'Assist' gas in the laser drilling of titanium, J. Laser Appl. 13 (5) (2001) 204–208.
[45] K.T. Voisey, Laser drilling of metals and ceramics, Ph.D. thesis, University of Cambridge, 2002.
[46] J. Murthy, R.E. Muller, V.V. Semak, M.H. McCay, Investigation of the drilling dynamics in Ti-6Al-4V using high speed photography, in: Proceedings of ICALEO'94, Orlando, FL, 1994, pp. 820–829.
[47] I. Barin, O. Knacke, Thermochemical Properties of Inorganic Substances, Springer, Berlin, 1973.
[48] D.D. Wagman, W.H. Evans, V.B. Parker, R.H. Schumm, I. Halow, S.M. Bailey, K.L. Churney, R.L. Nuttal, The NBS Tables of Chemical thermodynamic Properties, American Chemical Society and American Institute of Physics, Washington, 1982.
[49] D.R. Stull, H. Prophet, JANAF Thermochemical Tables, second ed., US Government Printing Office, Washington, 1971.
[50] J.N. Kamalu, W.M. Steen, The importance of gas flow parameters in laser cutting, in: K. Mukherjee, J. Mazumder (Eds.), Lasers in Metallurgy, AIME, New York, 1981, pp. 263–278.
[51] Y.S. Toulokian, P.E. Liley, S.C. Saxena, in: Y.S. Touloukian, C.Y. Ho (Eds.), Thermophysical Properties of Matter: Thermal Conductivity, vol. 3, IFI/Plenum, New York, 1970.
[52] Y.S. Toulokian, S.C. Saxena, P. Hestermans, in: T.S. Touloukian, C.Y. Ho (Eds.), Thermophysical Properties of Matter—Viscosity, vol. 11, IFI/Plenum, New York, 1970.
[53] P.E. LileyProperties of Nonmetallic Fluid Elements, McGraw-Hill/CINDAS Data Series on Material Properties, vol. III-2, McGraw-Hill, New York, 1981.